CMS Physics Analysis Summary

Contact: cms-pag-conveners-heavyions@cern.ch 2018/05/15

Production of prompt and nonprompt J/ψ mesons in jets in pp collisions at $\sqrt{s} = 5.02$ TeV

The CMS Collaboration

Abstract

The fragmentation of jets containing a J/ψ meson is studied in low pile-up pp data recorded in 2015, at a center-of-mass energy of $\sqrt{s} = 5.02$ TeV. The fraction of the jet transverse momentum $p_{\mathrm{T,jet}}$ taken by the J/ψ is measured for both prompt and nonprompt J/ψ mesons. The value of $p_{\mathrm{T,jet}}$ is restricted to the range of 25 – 35 GeV. The J/ψ mesons are measured above 3 and 6.5 GeV, in the endcap and barrel regions of the CMS detector, respectively. Whereas the results for nonprompt J/ψ are well-modeled by simulations using a Monte Carlo generator, the prompt J/ψ are found to be accompanied by a larger level of jet activity. The fraction of J/ψ mesons that are found to be inside a jet within the $p_{\mathrm{T,jet}}$ selection is also reported, and found to be larger than simulation, for both prompt and nonprompt J/ψ.

1 Introduction

The production of heavy quarkonia, such as J/ψ and Y mesons, in hadronic collisions remains far from being fully understood [1]. Among the various theoretical approaches, the non-relativistic QCD (NRQCD) effective field theory is able to reproduce the absolute differential production cross sections measured in collider experiments, in contrast to the Color Singlet Model (CSM) which predictions underestimate the magnitude of quarkonium production at large transverse momentum p_{T} [2]. However, NRQCD predicts that quarkonia are produced transversely polarized, which is not observed in data from the LHC [3–5]. Clearly the detailed parton dynamics responsible for the formation of heavy quark bound states remains elusive. In this respect, precise quarkonium production measurements – either single inclusive production or in association with other particles – can help narrow down the understanding of quarkonium formation in QCD.

Similar to the case of light hadron production, J/ψ hadronization dynamics can be studied by measuring the p_{T} fraction, $z \equiv p_{\mathrm{T,J/}\psi} / p_{\mathrm{T,jet}}$, carried by the J/$\psi$ meson detected inside a jet. The shape of the fragmentation pattern may be able to reveal the relative proportion of J/ψ produced directly in the hard partonic subprocess or by parton fragmentation, and hence to reveal the dominant subprocesses at work in J/ψ production. In addition, the production of nonprompt J/ψ, coming from b hadron decays, inside a jet should be sensitive to the fragmentation functions of quarks and gluons into b hadrons.

On top of its fundamental interest in QCD, the details of quarkonium hadronization has profound implications on the interpretation of J/ψ suppression observed up $p_{\mathrm{T}} \lesssim 50$ GeV in PbPb collisions at the LHC [6], since the fate of the color singlet and color octet components in the quark-gluon plasma (QGP) – possibly formed in the early stage of these collisions – should differ drastically. More explicitly, color octet states propagating in the plasma are expected to lose energy through medium-induced gluon radiation, leading to the quenching of high-p_{T} quarkonium production in heavy ion collisions with respect to pp collisions. On the contrary, compact color singlet states would not be sensitive to energy loss processes because of QCD color transparency. The similarity of the prompt J/ψ suppression pattern and that of jet and light hadrons has been highlighted recently [7]. The fragmentation of jets containing a nonprompt J/ψ meson is also of interest in heavy-ion collisions. In this case, the modification of the fragmentation pattern is sensitive quenching effects on b quark jets.

The fragmentation of jets into J/ψ was recently measured in pp collisions at $\sqrt{s} = 13\,\mathrm{TeV}$ by the LHCb Collaboration [8]. Their measurement, performed in the the pseudorapidity range $2.5 < \eta < 4.0$, and using jets of $p_{\mathrm{T}} > 20\,\mathrm{GeV}$, found that while the production of nonprompt J/ψ in jets is well-described by models, prompt J/ψ tend to be produced at much lower z than predicted by models. Here we report a similar measurement using an integrated luminosity of $\mathcal{L} = 27.39\ \mathrm{pb}^{-1}$ of 5.02 TeV pp data recorded with CMS. We report on the J/ψ production in jets as a function z, the fraction of the jets p_{T} taken by the J/ψ, using jets with $25 < p_{\mathrm{T}} < 35$ GeV and selecting J/ψ in two rapidity regions $0 < |y| < 1.6$ and $1.6 < |y| < 2.4$ for $6.5 < p_{\mathrm{T}} < 35$ GeV and $3.0 < p_{\mathrm{T}} < 35$ GeV, respectively. Both the prompt and nonprompt components of the J/ψ production are reported.

2 The CMS detector

The central feature of the CMS apparatus is a superconducting solenoid of 6 m internal diameter, providing a magnetic field of 3.8 T. Within the solenoid volume are a silicon pixel and strip tracker, a lead tungstate crystal electromagnetic calorimeter, and a brass and scintillator hadron

calorimeter, each composed of a barrel and two endcap sections. Forward calorimeters extend the coverage provided by the barrel and endcap detectors. Muons are measured in the pseudorapidity range $|\eta| < 2.4$ in gas-ionization detectors embedded in the steel flux-return yoke outside the solenoid, with detection planes made using three technologies: drift tubes, cathode strip chambers, and resistive-plate chambers. The hadron forward (HF) calorimeters use steel as an absorber and quartz fibres as the sensitive material. The two HF calorimeters are located 11.2 m from the interaction region, one on each side, and together they provide coverage in the range $2.9 < |\eta| < 5.2$. They also serve as luminosity monitors. Two beam pick-up timing detectors are located at 175 m on both sides of the interaction point, and provide information about the timing structure of the LHC beam. Events of interest are selected using a two-tiered trigger system [9]. The first level (L1), composed of custom hardware processors, uses information from the calorimeters and muon detectors to select events. The second level, known as the high-level trigger (HLT), consists of a farm of processors running a version of the full event reconstruction software optimised for fast processing. A more detailed description of the CMS detector, together with a definition of the coordinate system used and the relevant kinematic variables, can be found in Ref. [10].

The vertices are reconstructed with a deterministic annealing vertex fitting algorithm using all of the fully reconstructed tracks [11]. The physics objects used to determine the primary vertex are defined based on a jet finding algorithm [12, 13] applied to all charged tracks associated with the vertex, plus the corresponding associated missing transverse momentum. The reconstructed vertex with the largest value of summed physics object p_{T}^2 is taken to be the primary pp interaction vertex.

3 Data and object selections

3.1 Event selection

J/ψ mesons are reconstructed using their dimuon decay channel. The dimuon events were selected online by the L1 trigger system, requiring two tracks in the muon detectors with no explicit momentum threshold, in coincidence with a bunch crossing identified by beam pick-up timing detectors. No additional selection was applied by the HLT.

Simulated events are used to tune the muon selection criteria and the signal fitting parameters, as well as to correct for the acceptance, efficiency and p_{T} resolution. These samples are produced using PYTHIA 8.212 [14], propagated through the CMS detector with GEANT4 [15]. For the nonprompt simulation, b hadrons are decayed with EVTGEN 1.3.0 [16]. The prompt J/ψ is simulated unpolarized, a scenario in good agreement with pp measurements [3–5]. For nonprompt J/ψ, the polarization is the one predicted by EVTGEN, roughly $\lambda_\theta = 0.4$. The resulting events are processed through the trigger emulation and the event reconstruction sequences.

3.2 Muon selection

The muon reconstruction algorithm starts by finding tracks in the muon detectors, which are then fitted together with tracks reconstructed in the silicon tracker. Kinematic selections are imposed to single muons so that their combined trigger, reconstruction and identification efficiency stays above 10%. These selections are: $p_{\mathrm{T}} > 3.50\,\mathrm{GeV}$ for $|\eta| < 1.2$ and $p_{\mathrm{T}} > 1.89\,\mathrm{GeV}$ for $2.1 < |\eta| < 2.4$, linearly interpolated in the intermediate $|\eta|$ region. The muons are required to match the ones selected by the dimuon trigger, and *soft* muon selection criteria are applied to *global muons* (i.e. muons reconstructed using the combined information of the tracker and muon detectors), as defined in Ref. [17]. Matching muons to tracks measured in the silicon

tracker results in a relative p_T resolution for muons between 1 and 2% for a typical muon in this analysis [17]. In order to remove cosmic and in-flight decay muons, the transverse and longitudinal distances of approach to the measured vertex of the muons entering in the analysis are required to be less than 0.3 and 20 cm, respectively. The probability that the two muon tracks originate from a common vertex is required to be larger than 1%, lowering the background from b and c hadron semileptonic decays.

3.3 Jet selection

Jets are clustered using the anti-k_T algorithm, with R=0.4, from constituents created by the CMS particle-flow algorithm [18]. J/ψ candidates are input directly into the clustering, by replacing the daughter muons with the reconstructed J/ψ kinematics (using the Particle Data Group value of the J/ψ mass [19]). This procedure is applied to both reconstructed and generator level jets. Jets are calibrated using the same corrections derived for inclusive jets, as described in Ref. [20]. These corrections are only applied to the component of the jet p_T from particles other than the J/ψ itself, i.e., jet $p_T \times (1 - z)$. Since the J/ψ kinematics are already precisely measured from charged particle trajectories, no calibration is necessary. The p_T resolution of jets in simulation is smeared by 10% of its value to account for the difference in resolution in data and MC.

4 Signal extraction

Because of the long lifetime of b hadrons compared to that of J/ψ mesons, the separation of the prompt and nonprompt J/ψ components relies on the measurement of a secondary $\mu^+\mu^-$ vertex displaced from the primary collision vertex. The J/ψ mesons originating from the decay of b hadrons can be resolved using the pseudo-proper decay length [21] $\ell_{J/\psi} = L_{xyz}\, m_{J/\psi}\, c/|p_{\mu\mu}|$, where L_{xyz} is the distance between the primary and dimuon vertices, $m_{J/\psi}$ is the Particle Data Group world average value of the J/ψ meson mass (assumed for all dimuon candidates), and $p_{\mu\mu}$ is the dimuon momentum. Note that due to resolution effects and background dimuons the pseudo-proper decay length can take negative values. To measure the fraction of J/ψ mesons coming from b hadron decays (the so-called nonprompt fraction), the invariant mass spectrum of $\mu^+\mu^-$ pairs and their $\ell_{J/\psi}$ distribution are fitted using a two-dimensional (2D) extended unbinned maximum-likelihood fit. In order to obtain the parameters of the different components of the 2D probability density function (PDF), the invariant mass and the $\ell_{J/\psi}$ distributions are fitted sequentially prior to the final 2D fits, as explained below. These fits are performed for the different z bins, in each rapidity range.

The sum of two Crystal Ball functions [22], with different widths but common mean and tail parameters, is used to extract the nominal yield values from the invariant mass distributions. The tail parameters are fixed to the values obtained from simulation. The background is described by a polynomial function of order N, where N is the lowest value that provides a good description of the data, and is determined by performing a log-likelihood ratio test between polynomials of different orders, in each analysis bin, while keeping the tail and width ratio parameters fixed. The order of the polynomial is chosen in such a way that increasing the order does not significantly improve the quality of the fit. The order of the polynomial is 1 for all the analysis bins. The invariant mass signal and background parameters are obtained in an initial fit of the invariant mass distribution only and then fixed on the 2D fits of mass and $\ell_{J/\psi}$ distributions, while the number of extracted J/ψ mesons and background dimuons are left as free parameters.

The prompt, nonprompt, and background components of the $\ell_{J/\psi}$ distributions are parameterized using collision data and Monte Carlo (MC) simulated events, and the signal and back-

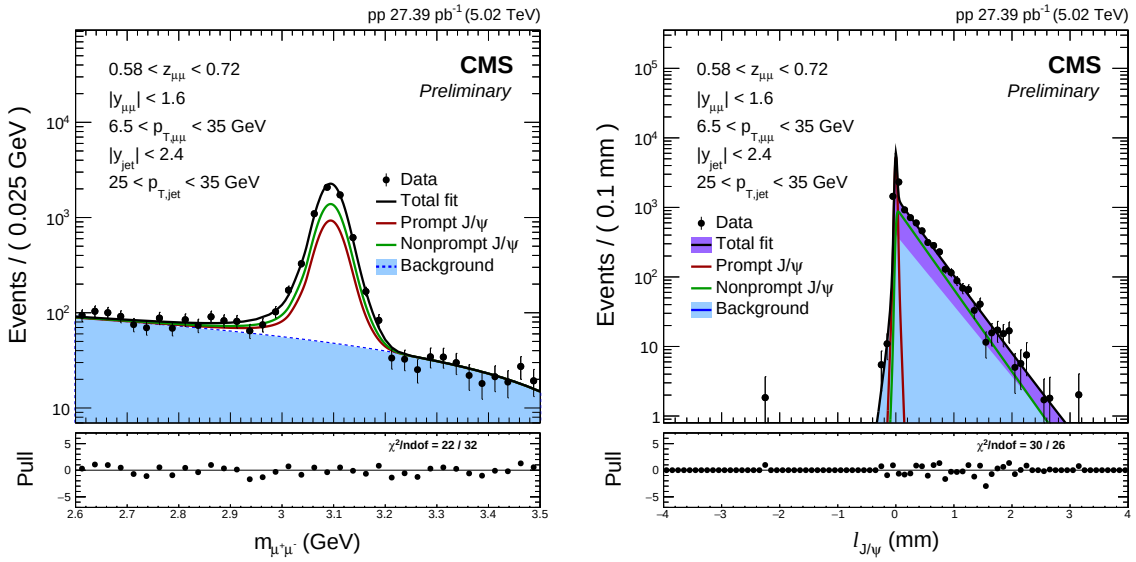

Figure 1: Invariant mass spectrum of $\mu^+\mu^-$ pairs (left) and pseudo-proper decay length distribution (right) in pp collisions for $0 < |y| < 1.6$, $6.5 < p_T < 35.0$ GeV. The result of the fit described in the text is also shown.

ground contributions unfolded with the ${}_s\mathcal{P}lot$ technique [23]. In the context of this analysis, this technique uses the invariant mass signal and background PDFs to discriminate signal from background in the $\ell_{J/\psi}$ distribution. The $\ell_{J/\psi}$ per-event uncertainty distributions of signal and background, provided by the reconstruction algorithm of primary and secondary vertices, are extracted from data and used as templates. The $\ell_{J/\psi}$ resolution, which depends on the $\ell_{J/\psi}$ uncertainty, is also obtained from the data by fitting the distribution of events with $\ell_{J/\psi} < 0$ with a combination of two Gaussian functions. All the resolution parameters are fixed in the 2D fits. The b hadron decay length is allowed to float freely in the fit, and it is initialized to the value extracted by fitting the $\ell_{J/\psi}$ distribution of nonprompt J/ψ mesons from a MC sample with an exponential decay function, at generator level. The $\ell_{J/\psi}$ distribution of background dimuons is obtained from fits to the data, using an empirical combination of exponential functions. The parameters of the $\ell_{J/\psi}$ background distribution are also fixed in the 2D fits. Finally, the number of extracted J/ψ mesons, the number of background dimuons and the nonprompt fraction are extracted from the 2D fits. An example of a 2D fit of the invariant mass and pseudo-proper decay length is shown in Fig. 1 for a representative analysis bin.

5 J/ψ acceptance and efficiency

Correction factors are applied to the results to account for detector acceptance, trigger, reconstruction, and selection efficiencies of the $\mu^+\mu^-$ pairs. The correction factors are computed as a function of the J/ψ p_T and rapidity in fine bins, and applied event-by-event to each J/ψ candidate. They are a mix of prompt and nonprompt corrections, mixed together using the b-fraction as a function of p_T, extracted from data in Ref. [24]. The acceptance times efficiency ($\mathcal{A} \times \varepsilon$) in a given bin is defined as the fraction of generated J/ψ mesons in that bin which are reconstructed and pass the analysis selection, and reflects the geometrical coverage of the CMS detector and the trigger, reconstruction, and selection efficiencies.

The individual components of the efficiency (tracking reconstruction, standalone muon reconstruction, global muon fit, muon identification and selection, and triggering) are also measured

using single muons from J/ψ meson decays in both simulated and collision data, using the *tag-and-probe* (T&P) technique [25, 26]. The values obtained from data and simulation are seen to differ only for the muon trigger efficiency and the ratio of the data over simulated efficiencies is used as a correction factor for the efficiency. The correction factor is at most 1.35 at the lowest single muon p_T and forward rapidity, but the p_T-integrated value of the correction is about 1.03. The other T&P efficiency components are compatible, hence only used as a cross-check, as well as to estimate systematic uncertainties.

6 Unfolding of p_T resolution

Migration across z bins, due to the finite jet p_T resolution, are corrected for using D'Agostini's iterative method [27], as encoded in the RooUnfold software package [28]. The unfolding is carried out in two dimensions, z and jet p_T, using the detector response derived from Monte Carlo simulations. To handle migration into the nominal jet p_T range from lower and higher p_T, the measurement is performed in two additional p_T bins: 15 – 25 and 35 – 45 GeV. The detector response matrices for prompt and nonprompt J/ψ at forward rapidity are shown in Fig. 2. For illustation, the plots show the same binning for the truth and measured axes. In practice, however, a finer binning is used along the truth axes to mitigate any bias coming from the mismodeling of the spectral shape in simulation. These matrices represent the probability for a jet in a given jet p_T and z bin, to migrate to any other bin. The unfolding is initiated starting from a prior that is flat in z. Three iterations are then carried out, after which the unfolding is quite convergent. The prior is then reinitialized, but this time reweighting its z distribution to match the output of the first 3 iterations. Overall three sets of three iterations are performed, as no gain in accuracy is observed using additional iterations.

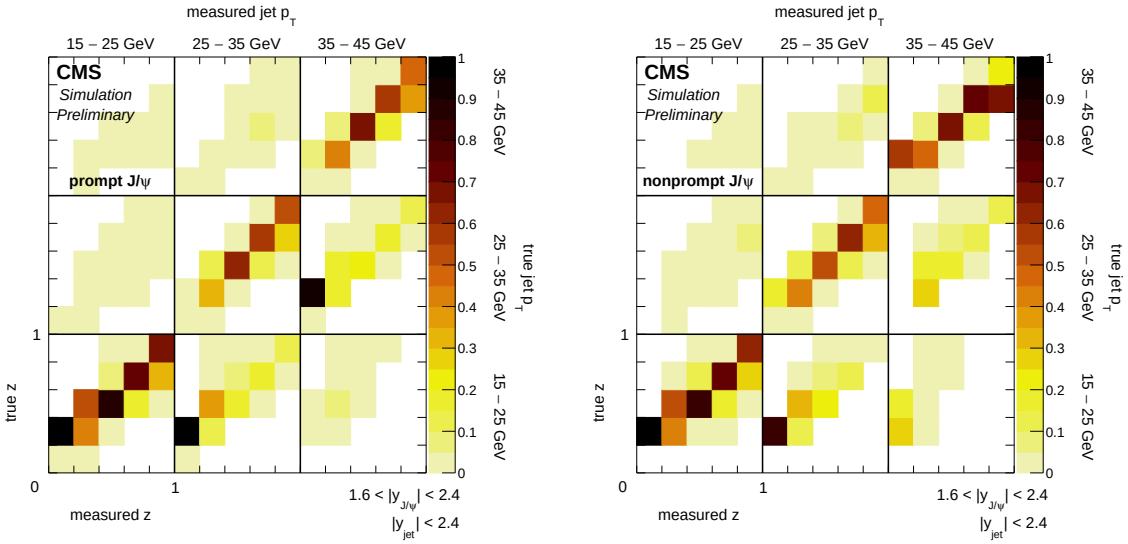

Figure 2: The four-dimensional detector-response matrices for prompt (left) and nonprompt J/ψ (right), as a function of jet p_T and z. The colors represent the bin-to-bin migration probabilities ranging from 0 (light yellow) to 1 (dark brown).

7 Systematic uncertainties

The systematic uncertainties in this measurement arise from the invariant mass signal and background fitting model assumptions, the parameterization of the $\ell_{J/\psi}$ distribution and the

$\mathcal{A} \times \varepsilon$ computation, as well as jet energy scale and resolution, and the unfolding procedure. Sytematic uncertainties vary with z. In the following discussion, we list their maximum values for illustration.

The systematic uncertainty due to each component of the 2D fits is estimated from the difference between the nominal value and the result obtained with the variations of the different components mentioned below, in the extracted number of prompt and nonprompt J/ψ mesons separately.

In order to determine the uncertainty associated with the invariant mass fitting procedure, the signal and background PDFs are independently varied, in each analysis bin. The signal shape uncertainty has two components. The first is obtained by leaving free at once all the parameters that were fixed in the nominal fits, with a certain constraint. The constraint for each parameter is determined from fits to the data, by leaving the corresponding parameter free, in different p_{T} and rapidity bins. The constraint is chosen as the root mean square of the parameter values obtained in the different bins. The second is obtained by using a different function for the signal shape: a Crystal Ball (CB) function plus a Gaussian function, with the CB tail parameters, again fixed from MC. The signal shape uncertainty yields a maximum value of 3.1% for the number of extracted prompt J/ψ mesons in forward rapidity. For the background model, the following changes are considered, while keeping the nominal signal shape. First, the log-likelihood ratio tests are done again with two variations of the condition required to choose the order of the polynomial function in each analysis bin. In this case, no dependence on the order of the polynomial chosen was observed, so no uncertainty is attributed to this variation. Also, the fitted mass range is varied from 2.6 – 3.5 GeV to 2.6 – 3.4 GeV. Finally the impact of the assumed shape for the background parameterisation is determined by using an exponential of a polynomial function. The dominant uncertainty in the background model arises from the assumed shape. The corresponding uncertainty reaches a maximum of 7.5% for prompt J/ψ in the forward rapidity region. The maximum of each of these variations, in each analysis bin and separately for the signal and the background, is taken as an independent systematic uncertainty.

For the $\ell_{\mathrm{J}/\psi}$ distribution fitting procedure, four independent variations of the different components entering in the 2D fits are considered. The total $\ell_{\mathrm{J}/\psi}$ uncertainty is the quadrature sum of these variations. For the $\ell_{\mathrm{J}/\psi}$ uncertainty distribution, instead of using the distributions corresponding to signal and background, the total distribution is assumed. The contribution to the systematic uncertainty reaches a maximum of 1.7% for nonprompt J/ψ at forward rapidity. The $\ell_{\mathrm{J}/\psi}$ resolution obtained from prompt J/ψ meson MC is used instead of that evaluated from data. The corresponding uncertainty is largest for the prompt fraction at forward rapidity where it reaches 2.1%. A nonprompt J/ψ meson MC template replaces the exponential decay function for the b hadron decay length. In this case, the maximum contribution of this source to the systematic uncertainty is 4.8% in the prompt J/ψ yield at mid rapidity. A template of the $\ell_{\mathrm{J}/\psi}$ distribution of background dimuons obtained from the data is used to describe the background, instead of the empirical combination of exponential functions. The largest impact of this variation is on the nonprompt J/ψ yield where it reaches 3.5%.

The uncertainties in the $\mathcal{A} \times \varepsilon$ determination are evaluated with MC studies, by applying the corrections with certain variations to the MC sample in the same way as they are applied to data. The variations include the statistical uncertainties of the corrections, the T&P scale factors and the mismodeling of the corrections. The corresponding uncertainty is obtained from the difference of the number of reconstructed J/ψ counted in each analysis bin using the nominal correction and the number obtained with the correction with a certain variation. The statistical

uncertainty on the correction due to the limited MC sample available are evaluated by randomizing the values in each bin of the correction following a binomial distribution. This uncertainty is at most 0.2% for prompt J/ψ. In addition, the systematic uncertainties in the T&P correction factors, arising from the limited data sample available and from the procedure itself, are taken into account, covering all parts of the muon efficiency: inner tracking and muon reconstruction, identification, and triggering. The dominant uncertainty in the T&P correction factors arises from muon reconstruction and reaches a maximum of 3.6% for prompt J/ψ in the forward rapidity range. The mismodeling of the $\mathcal{A} \times \varepsilon$ is taken into account by applying prompt and nonprompt corrections to the corresponding MC sample instead of using the mix of both. This uncertainty is at maximum for nonprompt J/ψ at forward rapidity where it reaches 3.4%.

An uncertainty of 2% and 10% is attributed the jet energy scale and resolution, respectively, based on Ref. [20]. The uncertainty on jet energy scale is applied by shifting the jet p_{T} and propagating the effect to the z distribution. This uncertainty is at most 8% at the lowest z in the forward rapidity, but it ranges from 0.4 to 5.8% at mid-rapidity. An uncertainty of 10% is attributed to the jet p_{T} resolution, which is applied by varying the data/MC scale factor on the resolution from 1.0 to 1.2, from its nominal value of 1.1. This uncertainty ranges from 0.8% to 3.6% for the prompt J/ψ, and it has the larges value of 8.5% at the higest z in the nonprompt forward rapidity.

The z distribution in prompt J/ψ MC provides a poor description of the data. An additional uncertainty is assigned to the prompt J/ψ jet energy scale to account for this. This uncertainty covers the difference between the prompt and nonprompt jet energy scales from simulation. This source of uncertainty is largest at high z, where it is 11.5% for forward rapidity and 6% for mid-rapidity.

The statistical uncertainty on the detector response is estimated by producing toy variations of the MC transfer matrices by smearing the bin contents by their statistical uncertainties. The uncertainty is largest at the lowest z in forward rapidity and it equals to 10.4%, but it ranges from 0.6% to 3.1% in mid-rapidity. The systematic uncertainty on the unfolding procedure is evaluated by varying the number of sets of iterations down to 2 and up to 4 from the nominal choice of 3. This uncertainty ranges from 0.8% to 4.1%.

The total uncertainty at mid-rapidity ranges from 1.9% to 10.5%, and in the forward rapidity from 2.4% to 21.1%, with the largest uncertainties occurring at low z.

8 Results and discussion

The self-normalized z distributions are presented for mid-rapidity and forward rapidity in Figs. 3 and 4, respectively. The prompt and nonprompt data show a qualitatively similar trend in each of the rapidity selections. A similar trend is observed in the PYTHIA 8 for nonprompt J/ψ, although the z distributions are slightly harder than the data. The trend for prompt J/ψ in PYTHIA 8, on the other hand, is very different than that observed in data. The z distribution is much too hard, indicating that the jet activity accompanying J/ψ mesons is underestimated. For the nonprompt case, the z distribution of the parent b hadron from PYTHIA 8 is also shown, which is peaked at much larger values of z compared to the daughter J/ψ. The apparent similarity of the prompt and nonprompt J/ψ in data, should therefore be interpreted with caution, as decay kinematics play a large role in the latter case.

While the jet activity around J/ψ mesons appears to be underestimated by PYTHIA, only a small fraction of J/ψ belong to jets in the selected p_{T} range of 25 to 35 GeV. This fraction of prompt

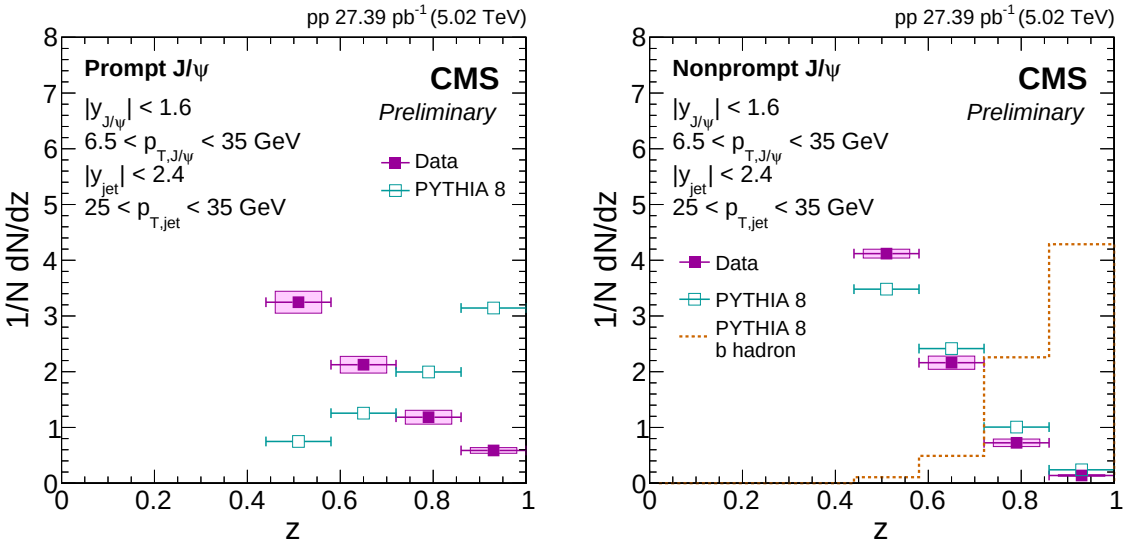

Figure 3: Self-normalized prompt (left) and nonprompt z distributions in the rapidity range $|y| < 1.6$, for pp data and PYTHIA 8. For the nonprompt case, the z distribution of the parent b hadron is also shown.

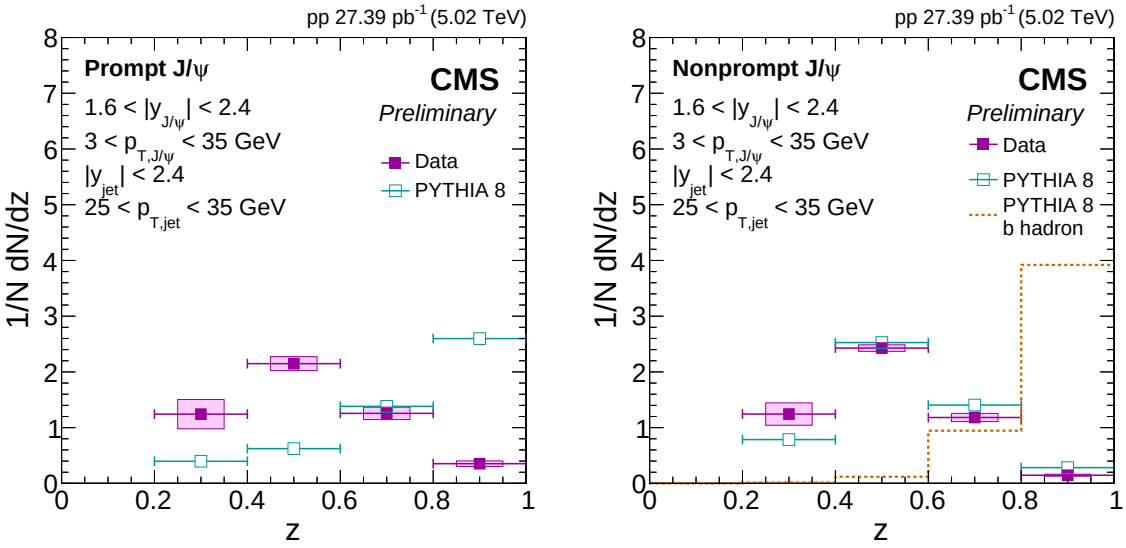

Figure 4: Self-normalized prompt (left) and nonprompt z distributions in the rapidity range $1.6 < |y| < 2.4$, for pp data and PYTHIA 8. For the nonprompt case, the z distribution of the parent b hadron is also shown.

and nonprompt J/ψ mesons in jets, as well as the data-to-MC ratio of these fractions, is shown in Fig. 5, for J/ψ above the minimum p_T threshold of 6.5 and 3 GeV, at mid- and forward rapidity, respectively. To evaluate this ratio, the numerator is taken by integrating the z distributions, but without applying the self-normalization. The jet energy scale and resolution uncertainties are correspondingly re-evaluated without the self-normalization. The other systematic uncertainties are treated as uncorrelated point-to-point, but are unaffected by the normalization. The denominator is evaluated by performing the 2D fitting procedure without any constraint on the associated jet. We find that the fraction of J/ψ produced in jets in the selected p_T range is underpredicted by PYTHIA 8 for both prompt and nonprompt J/ψ, for both rapidity selections. The nonprompt J/ψ show a larger jet fraction than is observed for prompt J/ψ. This suggests that J/ψ at lower values of p_T are less jet-like than nonprompt J/ψ. These J/ψ-in-jet fractions have not been studied before, to our knowledge, and provide complementary information to the z distributions that should prove useful for model comparisons.

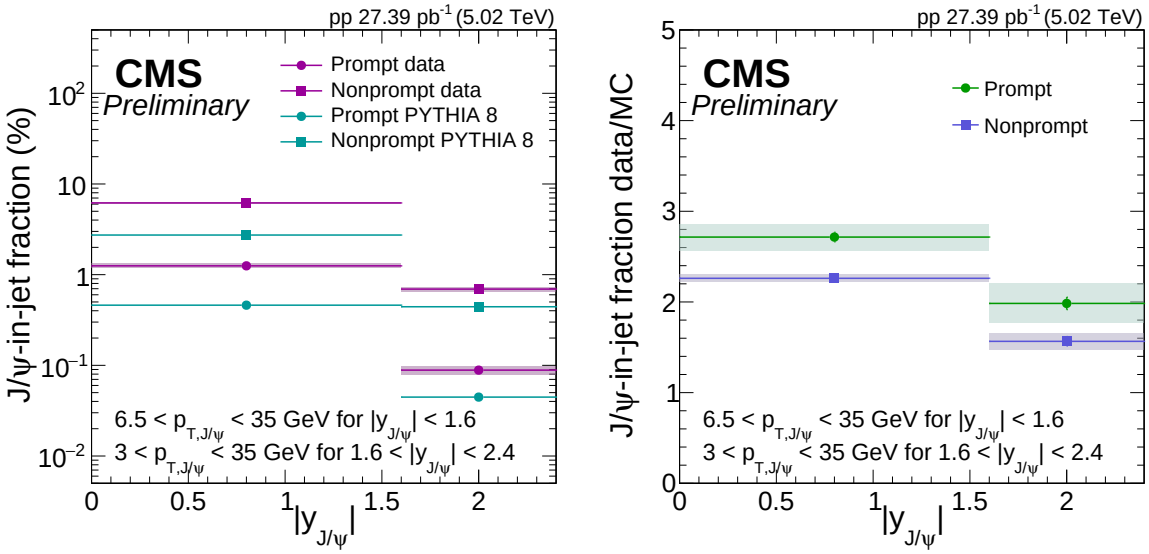

Figure 5: Left: The fraction of prompt and nonprompt J/ψ in jets of $25 < p_T < 35$ GeV in pp data and in PYTHIA 8, compared to the total number of J/ψ in the relevant the p_T interval, as indicated on the Figure. Right: The ratio of these J/ψ-in-jet fractions in data compared to simulation for prompt and nonprompt J/ψ.

9 Summary

In this analysis, the self-normalized z distributions for J/ψ mesons in jets of $25 < p_T < 35$ GeV, for both prompt and nonprompt J/ψ production, were reported. The distributions are presented above a lower threshold of 3 and 6.5 GeV, in the endcap ($1.6 < |y| < 2.4$) and barrel ($|y| < 1.6$) regions of the CMS detector, respectively. These results confirm the findings of LHCb [8], albeit in a different rapidity range and $\sqrt{s}$, namely that the nonprompt J/ψ production is reasonably well modeled by simulation, in this case PYTHIA 8, but that the prompt J/ψ production is qualiltatively different than predicted. Prompt J/ψ in jets tend to carry a smaller fraction of the jet momentum, indicating that they are less isolated than suggested by production models. In addition, we also report the fraction of the J/ψ mesons in jets, for jets in the same window of p_T (25 – 35 GeV), and for J/ψ meson above aforementioned lower p_T thresholds. This additional information should provide further constraints on models of J/ψ production.

References

[1] A. Andronic et al., "Heavy-flavour and quarkonium production in the LHC era: from protonproton to heavy-ion collisions", *Eur. Phys. J. C* **76** (2016) 107, doi:10.1140/epjc/s10052-015-3819-5, arXiv:1506.03981.

[2] N. Brambilla et al., "Heavy quarkonium: progress, puzzles, and opportunities", *Eur. Phys. J. C* **71** (2011) 1534, doi:10.1140/epjc/s10052-010-1534-9, arXiv:1010.5827.

[3] ALICE Collaboration, "J/ψ polarization in pp collisions at $\sqrt{s} = 7$ TeV", *Phys. Rev. Lett.* **108** (2011) 082001, doi:10.1103/PhysRevLett.108.082001, arXiv:1111.1630.

[4] CMS Collaboration, "Measurement of the prompt J/ψ and ψ(2S) polarizations in pp collisions at $\sqrt{s} = 7$ TeV", *Phys. Lett. B* **727** (2013) 381, doi:10.1016/j.physletb.2013.10.055, arXiv:1307.6070.

[5] LHCb Collaboration, "Measurement of J/ψ polarization in pp collisions at $\sqrt{s} = 7$ TeV", *Eur. Phys. J. C* **73** (2013) 2631, doi:10.1140/epjc/s10052-013-2631-3, arXiv:1307.6379.

[6] F. Arleo, "Quenching of Hadron Spectra in Heavy Ion Collisions at the LHC", *Phys. Rev. Lett.* **119** (2017) 062302, doi:10.1103/PhysRevLett.119.062302, arXiv:1703.10852.

[7] M. Spousta, "On similarity of jet quenching and charmonia suppression", *Phys. Lett. B* **767** (2017) 10, doi:10.1016/j.physletb.2017.01.041, arXiv:1606.00903.

[8] LHCb Collaboration, "Study of J/ψ production in jets", *Phys. Rev. Lett.* **118** (2017), no. 19, 192001, doi:10.1103/PhysRevLett.118.192001, arXiv:1701.05116.

[9] CMS Collaboration, "The CMS trigger system", *JINST* **12** (2017) P01020, doi:10.1088/1748-0221/12/01/P01020, arXiv:1609.02366.

[10] CMS Collaboration, "The CMS experiment at the CERN LHC", *JINST* **3** (2008) S08004, doi:10.1088/1748-0221/3/08/S08004.

[11] CMS Collaboration, "Description and performance of track and primary-vertex reconstruction with the CMS tracker", *JINST* **9** (2014) P10009, doi:10.1088/1748-0221/9/10/P10009.

[12] M. Cacciari, G. P. Salam, and G. Soyez, "The anti-k_t jet clustering algorithm", *JHEP* **04** (2008) 063, doi:10.1088/1126-6708/2008/04/063, arXiv:0802.1189.

[13] M. Cacciari, G. P. Salam, and G. Soyez, "FastJet user manual", *Eur. Phys. J. C* **72** (2012) 1896, doi:10.1140/epjc/s10052-012-1896-2.

[14] T. Sjöstrand et al., "An Introduction to PYTHIA 8.2", *Comput. Phys. Commun.* **191** (2015) 159, doi:10.1016/j.cpc.2015.01.024, arXiv:arXiv:1410.3012.

[15] GEANT Collaboration, "GEANT4 — A simulation toolkit", *Nucl. Instrum. Meth. A* **506** (2003) 250, doi:10.1016/S0168-9002(03)01368-8.

[16] D. J. Lange, "The EvtGen particle decay simulation package", *Nucl. Instrum. Meth. A* **462** (2001) 152, doi:10.1016/S0168-9002(01)00089-4.

[17] CMS Collaboration, "Performance of CMS muon reconstruction in pp collision events at $\sqrt{s} = 7$ TeV", *JINST* **7** (2012) P10002, doi:10.1088/1748-0221/7/10/P10002, arXiv:1206.4071.

[18] CMS Collaboration, "Particle-flow reconstruction and global event description with the cms detector", *JINST* **12** (2017) P10003, doi:10.1088/1748-0221/12/10/P10003, arXiv:1706.04965.

[19] Particle Data Group Collaboration, "Review of Particle Physics", *Chin. Phys. C* **40** (2016) 100001.

[20] CMS Collaboration, "Jet energy scale and resolution in the CMS experiment in pp collisions at 8 TeV", *JINST* **12** (2017) P02014, doi:10.1088/1748-0221/12/02/P02014, arXiv:1607.03663.

[21] ALEPH Collaboration, "Measurement of the anti-B^0 and B^- meson lifetimes", *Phys. Lett. B* **307** (1993) 194, doi:10.1016/0370-2693(93)90211-Y. [Erratum: Phys. Lett. B 325 (1994) 537].

[22] M. J. Oreglia, "A Study of the Reactions $\psi(2S) \to \gamma\gamma\psi$", 1980.

[23] M. Pivk and F. Le Diberder, "${}_s\mathcal{P}lot$: a statistical tool to unfold data distributions", *Nucl. Instrum. Meth. A* **555** (2005) 356, doi:10.1016/j.nima.2005.08.106, arXiv:physics/0402083.

[24] CMS Collaboration, "Measurement of prompt and nonprompt charmonium suppression in PbPb collisions at 5.02 TeV", *Submitted to: Eur. Phys. J. C* (2017) arXiv:1712.08959.

[25] CMS Collaboration, "Measurements of inclusive W and Z cross sections in pp collisions at $\sqrt{s} = 7$ TeV", *JHEP* **01** (2011) 080, doi:10.1007/JHEP01(2011)080, arXiv:1012.2466.

[26] CMS Collaboration, "Suppression of non-prompt J/ψ, prompt J/ψ, and Y(1S) in PbPb collisions at $\sqrt{s_{\mathrm{NN}}} = 2.76$ TeV", *JHEP* **05** (2012) 063, doi:10.1007/JHEP05(2012)063, arXiv:1201.5069.

[27] G. DAgostini, "A multidimensional unfolding method based on bayes theorem", *Nucl. Instrum. Meth. A* **362** (1995) 487, doi:10.1016/0168-9002(95)00274-x.

[28] T. Adye, "Unfolding algorithms and tests using roounfold", arXiv:1105.1160.